Structural Durability & Health Monitoring

Tech Science Press

Doi:10.32604/sdhm.2025.076570

ARTICLE

Structural Response Analysis of Existing Metro Stations under Simultaneous Excavation of Adjacent Foundation Pits and Tunnels

Jun Wang[1], Qian Fang[1,*], Weiguo He[2], Yanxin Chen[1] and Qizhao You[1]

[1]Key Laboratory of Urban Underground Engineering of Ministry of Education, Beijing Jiaotong University, Beijing, 100044, China
[2]China Railway Liuyuan Group Co., Ltd., Tianjing, 300308, China

*Corresponding Author: Qian Fang. Email:qfang@bjtu.edu.cn

Received: 22 November 2025; Accepted: 18 December 2025; Published: 18 May 2026

ABSTRACT: This study presents a comprehensive investigation into the deformation mechanisms of existing metro stations subjected to the simultaneous construction of adjacent foundation pits and underground tunnels. A refined three-dimensional numerical modeling framework is developed to simulate the entire construction process, capturing the complex interactions between excavation activities and station structures. The modeling encompasses deep excavation, side-crossing, and overcrossing passage construction, and the staged installation of support systems. Six construction schemes, varying in excavation sequence, interlayer thickness (clear distance), and passageway layout, are systematically analyzed. Field monitoring data are incorporated to validate the numerical models, enhancing the reliability of the results. The analysis identifies the construction sequence as the primary factor influencing station deformation. Specifically, the strategy of constructing passageways first, followed by excavation of the interchange hall, effectively reduces both vertical and horizontal displacements by leveraging the early-stage portal-frame reinforcement effect. Increasing the clear distance between new structures and the existing station helps mitigate construction-induced deformation, although the benefits plateau beyond a certain threshold. Sensitivity analysis shows that overcrossing passages are most sensitive to variations in clear distance, followed by foundation pits and side-crossing tunnels. Additionally, the spatial positioning of passageways significantly impacts deformation magnitude and propagation. Passageways near expansion joints cause the greatest uplift, while those placed at mid-span experience minimal disturbance due to enhanced structural stiffness. This research provides a quantitative understanding of metro station deformation under concurrent construction activities and offers practical insights for optimizing excavation sequences, structural layouts, and interlayer spacing. The findings contribute to ensuring structural safety and minimizing risks in densely built urban metro environments.

KEYWORDS: Tunnel; foundation pit; crossing project; expand station; numerical simulation

1 Introduction

In recent years, the shield tunneling method has become the preferred approach for constructing urban metro tunnels due to its high efficiency, minimal ground disturbance, and adaptability [1,2]. However, when stations are closely spaced or when tunnels pass through densely built urban areas, the economic benefits of continuous shield tunneling are limited, and construction complexity increases. To address these challenges, a new station construction method has been proposed. This approach involves first constructing a small- or medium-section pilot tunnel and then expanding it to form the main station cavern. It helps reduce traffic disruption, minimize surface disturbance, and improve construction safety. Although this method has been

applied in cities like Tokyo, Seoul, and several Chinese locations, systematic studies on its impact on existing metro structures are limited [3–7].

As metro networks become denser in urban cores, new underground works, such as tunnels, foundation pits, and station expansions, are increasingly likely to intersect or approach existing stations or tunnels, creating complex interaction mechanisms. Most studies have focused on the effects of individual construction activities, such as the deformation and force redistribution caused in existing tunnels by excavation pits [8–10], or the impact on stations from new tunnels under various overburden and clearance conditions [11]. Excavation pits, for instance, significantly alter the surrounding stress field, causing horizontal displacements, uplift, and differential settlement, which affect adjacent metro structures [11–14]. Research has shown that deformation on the tunnel side closer to the pit is much larger than on the far side, with this response closely related to excavation depth and location [15]. Field observations report horizontal tunnel displacements of up to 12–13.5 mm and vertical deformation between 4–8 mm, all within safety limits [16,17]. As excavation progresses, tunnel loading shifts from symmetric to eccentric, leading to more complex deformation patterns, with larger bending moments on the far side [16]. In some cases, existing stations have experienced simultaneous settlement (6 mm) and uplift (up to 13 mm) [18]. The impact zone of an excavation pit typically extends 1.5 times its depth, with effects diminishing beyond this range [19–21], and numerical simulations predict deformation patterns with minimal deviation (5.26%) [22].

When new tunnels cross existing ones, different alignment configurations lead to significantly different mechanical responses. Vertical undercrossings generally result in manageable deformation of existing structures [23], while parallel undercrossings over short distances cause greater deformation, often requiring clearance to be controlled within 1–1.5 D (where D is tunnel diameter) [24,25]. Oblique crossings, on the other hand, can induce asymmetric deformation and local torsion, leading to more complex structural responses [26,27]. Shield tunneling disturbances typically occur in three phases: approaching, crossing, and departure, and may also involve pre-settlement from ground improvement [28]. The mechanical response of existing tunnels depends on clearance, crossing angle, construction control, and ground properties. For example, doubling tunnel clearance only reduces surface settlement by about 30%, showing that clearance alone is insufficient to control deformation effectively [25,29]. Small-angle crossings can result in approximately 33% more settlement than vertical crossings [29,30], and parameters like friction angle and cover thickness can influence crown settlement and stress distribution by over 20% [31]. Thus, evaluating the combined effects of multiple factors is essential for accurately predicting structural responses in complex urban environments.

From a spatial perspective, different excavation positions can induce three primary deformation modes in existing tunnels: settlement, transition, and uplift zones [32]. Lateral excavation typically causes lateral settlement, while excavation above the tunnel tends to induce uplift [33]. When a tunnel lies below the excavation bottom, the induced stress is smaller, and the impact zone is more concentrated [34]. The structural continuity between a station and adjacent tunnels leads to a whip effect, influencing tunnel displacement, shear force, and rotation, with effects diminishing with distance [35]. In dense urban settings, multiple construction activities, such as shield tunneling, cross-passage enlargement, and foundation pit excavation proximity to existing stations, often occur simultaneously or in succession, creating multi-stage disturbances. However, studies on the combined impact of such disturbances on existing stations remain limited, and current findings do not fully address risk control and optimized design needs for underground spaces in highly developed urban areas. Although extensive studies have examined the effects of deep excavations, tunnel undercrossings, and mined enlargements on existing metro structures, these investigations typically consider each disturbance source independently. Newly constructed foundation pits and mined cross-passages often intersect or approach existing lines in an alternating or overlapping manner,

generating coupled and sequential disturbance effects that cannot be captured by single-source analyses. The mechanisms associated with such multi-phase interactions, combining pit-induced unloading with tunnel-induced stress redistribution, remain largely unexplored. This study addresses this gap by focusing on the deformation response of an existing metro station subjected to the successive construction of both a new foundation pit and mined tunnels, providing an integrated assessment that reflects the increasingly complex construction scenarios encountered in modern metro systems.

To address this, this study focuses on a typical scenario: the construction of a new foundation pit and mined cross-passage adjacent to an existing station. A refined FLAC3D numerical model is developed to simulate the entire "ground–structure–construction" process, validated with field monitoring data. Parametric analyses are then conducted to assess the effects of construction sequence, horizontal and vertical clearances, and cross-passage spatial positioning. The contributions of these factors to vertical uplift, horizontal displacement, and internal forces in the existing station are systematically evaluated.

2 Mechanisms of Multiple Underground Structures Adjacent to Existing Subways

As urban rail transit systems expand rapidly, the shield tunneling method has become the preferred technique for metro construction due to its high excavation efficiency, stable quality, minimal ground disturbance, and strong safety performance. In practice, however, several limitations have been identified. The relatively short tunneling distances common in dense cities reduce shield efficiency, while shield launching and retrieval may induce ground disturbance and pose risks to nearby facilities. When a shield machine must pass through existing or planned station boxes, additional shafts or temporary structures are often required, further complicating construction.

To overcome these challenges, large-diameter shield tunneling has been increasingly adopted for one-pass excavation of station caverns. While this method reduces surface disruption and construction interfaces, auxiliary structures such as concourses and cross-passages are typically constructed afterward using mined or cut-and-cover methods. These auxiliary excavations are widely recognized as important sources of localized unloading and stress redistribution, which must be considered when evaluating the interaction between new underground works and existing metro facilities.

In general, new underground structures adjacent to existing stations can be categorized into two typical configurations (Fig. 1): (1) interaction between deep foundation pits and existing stations, including adjacent or underpassing excavations; (2) the influence of mined tunnel-type structures, such as overpassing or side-crossing passages.

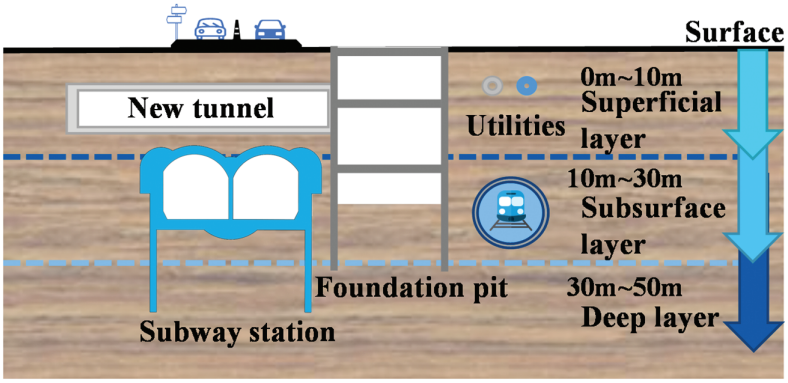

Figure 1: Schematic diagram of tunnel and foundation pit to existing subway station

Most existing studies address these two disturbance types separately. However, systematic research on their combined effects remains limited, despite their increasing occurrence in densely built urban areas. Understanding the deformation patterns and interaction mechanisms under multi-source disturbances is therefore essential for guiding risk control and construction planning for modern metro projects.

3 Numerical Model Development and Engineering Validation

3.1 Overall Approach and Modeling Procedure

To evaluate the deformation and mechanical response of an existing metro station under the combined influence of a new foundation pit and mined cross-passages, a comprehensive three-dimensional numerical model is developed using the FLAC3D finite-difference program. The model simulates the entire sequence of ground, existing structures, new structures, and construction activities, balancing engineering accuracy with computational efficiency. Key principles and considerations are outlined as follows:

(1) Geological strata and mechanical properties

Discretization of soil layers: Eight-node solid elements are used to discretize the ground mass, ensuring the continuity of stress and strain fields within the soil.

Material model: The Mohr–Coulomb elastic–plastic model is adopted to simulate soil behavior, as it adequately captures the strength and failure characteristics of soft clay, silt, sand, and clayey soils commonly encountered in metro construction. In the present analysis, strain-softening and dilatancy effects are not explicitly considered. Instead, soil layer parameters are selected based on empirical ranges and calibrated against field monitoring data to ensure that the overall deformation and internal-force responses of the metro station are reasonably represented.

(2) Soil–structure interaction modeling

Initial stress field: The initial *in-situ* stress state is generated under self-weight. For soft-soil areas, lateral earth pressure is corrected using the at-rest coefficient K_0.

Interfaces: Interface elements are inserted between the soil and both existing and newly constructed structures to simulate sliding, friction, and opening–closing behavior. This prevents unrealistically rigid bonding, which may lead to uneven stress distribution or distorted plastic zones.

Composite structural systems: For structural systems composed of diaphragm walls, primary linings, and internal columns, a common-deformation assumption is adopted between the soil and structural components, while allowing nonlinear relative deformation through interfaces between different components.

Deformation joints: Expansion or deformation joints are explicitly modeled using solid elements, allowing structural segments on both sides to deform independently.

(3) Initial stress field and boundary conditions

Initial stress state: The initial stress field is computed from self-weight, supplemented with static earth pressure calculated using K_0 for soft soils.

Boundary size: The horizontal extent of the numerical model is set to at least 3–5 times the excavation width to minimize boundary effects [36]. The bottom boundary extends to at least 2–3 times the excavation depth, while the top boundary coincides with the ground surface to ensure accurate representation of the overburden.

Boundary constraints: Three-directional displacement constraints are applied at the base. Normal displacement constraints are imposed on the lateral boundaries to represent a semi-infinite ground mass, while the ground surface remains free.

(4) Simulation of construction processes

Soil excavation: The stress release of the surrounding rock during tunnel construction is modeled in a stepwise manner. Initially, 60% of the *in-situ* stress is released during tunnel excavation. After completion of the initial lining, an additional 20% stress release is applied, followed by another 20% release upon completion of the secondary lining, resulting in a total stress release of 100% at the end of construction [37]. This staged stress release reflects the sequential unloading process and the interaction between excavation and lining installation.

Structural installation: Primary linings and temporary supports are activated segment by segment. For top-down construction, structural elements are activated sequentially from top to bottom, with corresponding layers of soil unloading applied progressively.

3.2 Model Parameters and Basis for Constitutive Selection

Material parameters are selected based on a three-level verification principle: geotechnical investigation results, statistical data from similar projects, and recommended ranges from codes, ensuring realistic and reliable parameter values.

(1) Soil parameters

Basic indicators such as natural density, void ratio, and natural water content are obtained from the site investigation report. Shear strength parameters are determined from laboratory triaxial, consolidation, and direct shear tests. Elastic modulus is corrected using empirical correlations or plate loading test results. Poisson's ratio is assigned according to typical values for corresponding soil types.

(2) Structural parameters and constitutive models

Segmental lining of shield tunnels: Modeled with solid elements as linear-elastic concrete.

Primary support: Simulated using solid elements representing shotcrete.

Beams and central columns: Constructed from concrete and modeled with solid elements.

Diaphragm walls and jet-grouted columns: Diaphragm walls are modeled as linear-elastic concrete solid elements. Temporary steel struts are modeled using beam elements with axial stiffness EA.

(3) Interface parameters

Interfaces between soil and structures follow the Coulomb friction model, with parameters including:

Normal stiffness kn and shear stiffness ks. Interface friction coefficient tan φ_c. Cohesion c represents the bonding capacity between the structure and the surrounding soil.

3.3 Engineering Background and Project

Gaojiayuan Station, located in Chaoyang District, Beijing, is a single-level, side-platform underground station created through large-diameter shield-driven enlargement. The concourse and platform levels are separated and connected via multiple mined cross-passages. The station's base slab is situated about 25 m deep, within Quaternary deposits of alternating silt, sand, and silty clay, with relatively uniform variations in overburden and bedrock profile. To support transfer functions, the new development includes two main components: a three-level transfer hall foundation pit, constructed using a combination of cut-and-cover and top-down methods, located parallel to and adjacent to the existing station, and a series of mined cross-passages at varying depths. These cross-passages cross above, beside, or beneath the existing station, forming a complex spatial system along with the transfer hall and platform.

The new structures are situated very close to the existing station, with the minimum clearance between them being less than 5 m. This tight spatial arrangement and the combined temporal interaction during construction are key aspects of this study. A typical layout of the foundation pit, station, and cross-passages is shown in Fig. 2. The project includes a total of fourteen cross-passages, with overpassing, oblique, and underpassing configurations. These passages, generally rectangular or horseshoe-shaped, are constructed using the mining method. Local vertical segments are excavated with the pilot-shaft method.

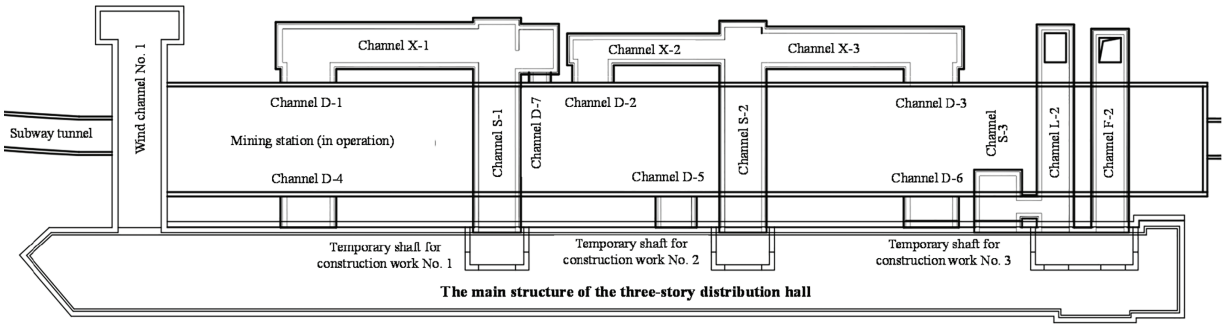

(a) Relative position between interchange hall and metro station structure

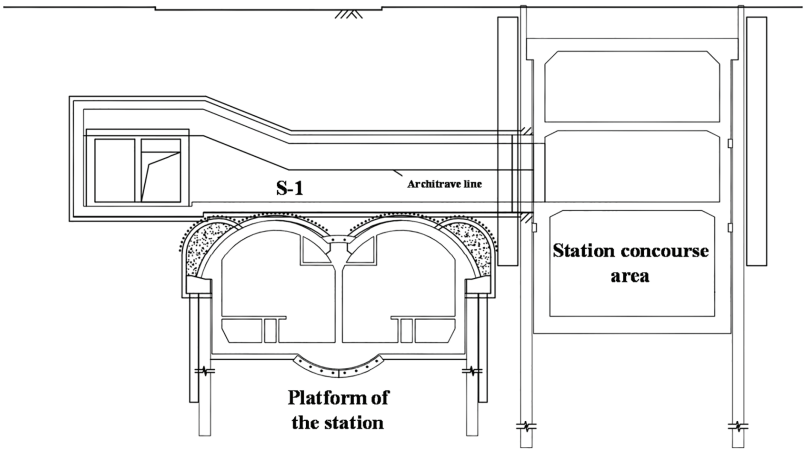

(b) Structural cross-section

Figure 2: Structural section drawing interchange hall and metro station structure

According to the geotechnical investigation, the site is composed mainly of alternating silt, silty clay, and medium-to-coarse sand, with a maximum exploration depth of approximately 51 m. The physical and mechanical properties of the major soil layers are summarized in Table 1, while a representative geological profile and passage layout are shown in Fig. 3.

Table 1: Physical and mechanical parameters and layer thickness of each layer

Soil layer	Thickness/m	Density/(kg/m^3)	Young's modulus/MPa	Cohesion/kPa	Internal friction angle/°	Poisson's Ratio
Silty soil fill	1.6	1750	6	5	10	0.35
Silty soil	7.3	1960	21	18	25	0.31

(Continued)

Table 1 (continued)

Soil layer	Thickness/m	Density/(kg/m^3)	Young's modulus/MPa	Cohesion/kPa	Internal friction angle/°	Poisson's Ratio
Medium-coarse sand	6.7	2050	45	0	38	0.29
Sandy clay	8.9	1950	23	32	18	0.31
Silty soil	5.8	1960	21	18	24	0.31
Sandy clay	3.3	1960	21	18	24	0.31
Medium-coarse sand	8.5	2050	46	0	35	0.29
Sandy clay	4	1980	16	35	20	0.31

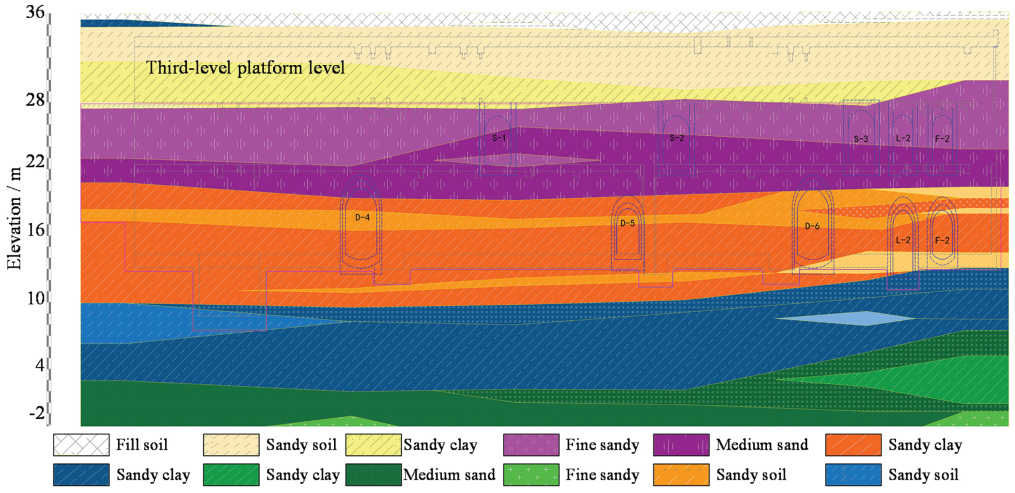

Figure 3: Geological profile and location map of the communication passage

The properties of the interfaces between the soil layers and the concrete structure used in the numerical model are shown in Table 2. For each soil layer, the normal stiffness (k_n) and shear stiffness (k_s) of the interface are estimated based on the soil's elastic modulus, following common practice for interface elements to avoid excessive penetration while maintaining numerical stability. The interface cohesion (c_{int}) and friction angle (ϕ_{int}) are set as a fraction of the corresponding soil properties, reflecting the typically weaker strength of soil–structure contacts observed in direct shear tests.

Table 2: Parameters of the interface between soil and structure

Soil layer	Normal stiffness/GPa	Shear stiffness/GPa	Cohesion/kPa	Friction angle/°
Silty soil fill	11	1.1	3	13
Silty soil	12	3.5	9	13

(Continued)

Table 2 (continued)

Soil layer	Normal stiffness/GPa	Shear stiffness/GPa	Cohesion/kPa	Friction angle/°
Medium-coarse sand	23	6.1	0	18
Sandy clay	12	3.4	16	9
Silty soil	13	3.2	9	13
Sandy clay	13	3.1	9	10
Medium-coarse sand	23	6.2	0	18
Sandy clay	12	2.3	17	11

In summary, this project serves as a typical example of multiple newly constructed underground structures interacting closely with an existing metro station. It features a complex structural system, overlapping construction activities, and varied geological conditions, making it an ideal case for validating numerical analyses and studying deformation-response mechanisms. The construction processes of the mined cross-passages and the cut-and-cover interchange hall are modeled in detail. The model dimensions and mechanical parameters of the strata beneath Gaojiayuan Station are summarized in Table 3. Boundary conditions are determined by considering both the soil disturbance caused by excavation and the need for computational efficiency. The model extends horizontally three times the excavation width on each side of the station, with the upper boundary set at the ground surface and the lower boundary extending three times the height of the station enlargement. In the longitudinal direction, the model extends three times the enlarged station width. The resulting model measures 340 m in length, 170 m in width, and 80 m in height. Normal displacement constraints are applied to the four vertical boundaries and the bottom. The model is shown in Fig. 4, with the axial definition used in subsequent analyses illustrated in Fig. 4b.

Table 3: Material parameter values of the model structure

Structural name	Young's modulus/GPa	Poisson's ratio	Density kg/m^3	Friction angle/°	Cohesion/kPa
Prefabricated shield segments	34.5	0.2	2500	—	—
Initial support	28	0.2	2300	—	—
Beam-column-base slab	32.5	0.2	2500	—	—
Temporary support	210	0.2	7800	—	—
Earth wall	20	0.3	2100	—	—

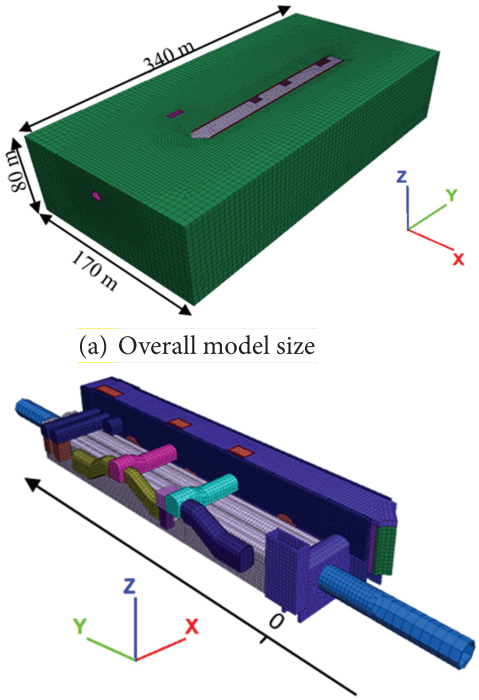

(a) Overall model size

(b) Structural model diagram

Figure 4: Numerical calculation model

The existing metro tunnels are built using shield tunneling with C50 precast concrete segments, which are modeled as solid elements. The segment lining has a thickness of 0.50 m, and an equivalent interface is introduced between the lining and the surrounding soil to maintain mechanical continuity. The initial supports for the station and cross-passages consist of C25 shotcrete, with a typical thickness of 0.25–0.35 m. For the open-cut and cut-and-cover sections, diaphragm walls (0.8 m thick, C30 concrete) are used for the side walls. The base and intermediate slabs are constructed with C40 reinforced concrete, with thicknesses ranging from 0.8 to 1.2 m depending on location and loading conditions.

3.4 Model Reliability Verification and Comparative Analysis

To verify the reliability of the numerical model and its ability to capture the actual structural response of the existing station during the construction of the new foundation pit and interchange passages, a comprehensive field monitoring system is employed for comparison. Based on the spatial relationships between the existing structures (station and running tunnels) and the new facilities, a total of 20 monitoring sections are arranged along the longitudinal extent of the station. Monitoring points are placed at key locations, including the station structure, running tunnel linings, and track slabs. Specifically, 52 vertical displacement points (on structures), 27 horizontal displacement points (on structures), and 80 vertical displacement points (on the track system) are installed.

The layout and arrangement of the monitoring points are shown in Fig. 5, covering the influence zones of the construction of new mined passages S-1, S-2, L-2, F-2, and the cut-and-cover foundation pit.

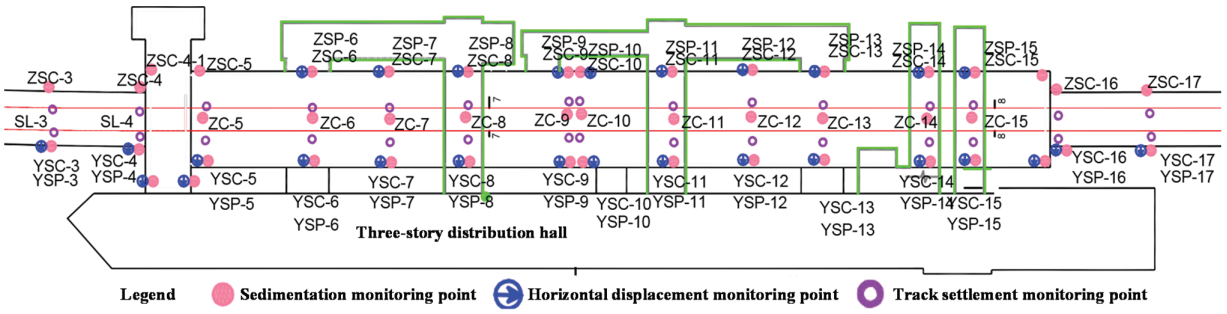

Figure 5: Station measurement point layout diagram

To ensure comprehensive validation of the model, this study uses a multi-source comparison framework, combining field monitoring data with numerical simulation. By comparing measured deformations with simulated results at the same construction stages, the model's ability to replicate soil disturbance, structural responses, and staged excavation effects is evaluated.

Monitoring results indicate that, during the construction of the new cross-passages, the existing station experienced slight heave, mainly due to the unloading effect from the mined excavation. Taking the S-1 passage as an example, Fig. 6 compares the longitudinal deformation curves from field monitoring and numerical simulation after the completion of S-1. The Pearson correlation coefficients between the measured and numerically simulated structural deformations of the left and right lines are 0.898 and 0.931, respectively. Both the simulation and field measurements show that the right tunnel experienced more heave than the left tunnel, with the maximum deformation occurring near the over-crossing location of S-1. This confirms the model's ability to capture the asymmetric disturbance induced by the new passage. The deformation patterns are highly consistent, with good agreement in peak positions and deformation gradients. Although the simulated values are slightly lower than the measured ones, the discrepancies are within acceptable engineering limits, suggesting that the model accurately represents key factors such as consolidation state, soil improvement, and construction sequencing.

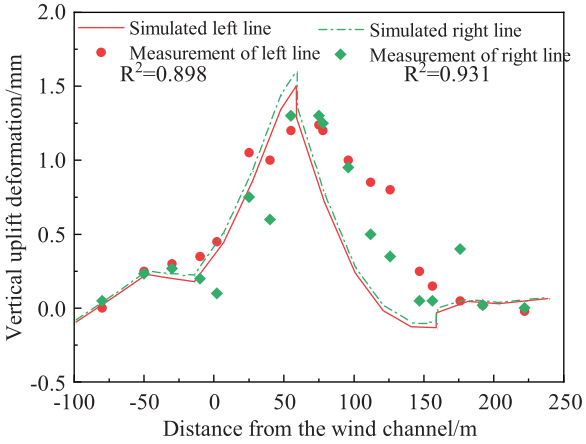

Figure 6: Comparison of measured and simulated deformation curves

4 Influence Factors and Response Mechanisms of Foundation Pits and Tunnels Adjacent to Existing Metro Stations

4.1 Deformation Responses under Different Construction Sequences

When a new foundation pit and multiple mined tunnels are constructed in an overlapping manner, the construction sequence directly alters the soil unloading path, the structural force-transfer mechanism, and the degree of disturbance imposed on the existing metro station. To systematically evaluate the response of the existing station under different construction arrangements, the construction process is categorized into two major sequence types: Type A (construct the interchange hall first, then the mined passages) and Type B (construct the mined passages first, then the interchange hall). In practical metro interchange construction, these two sequences represent the most typical and feasible engineering strategies. They produce fundamentally different unloading paths and structural response mechanisms, making them suitable for representative comparison. Although a simultaneous excavation of the foundation pit and mined tunnels could be conceived as another option, such an arrangement requires a substantially larger excavation volume, induces stronger ground disturbance, and is therefore seldom adopted in practice. For this reason, the present study concentrates on the two commonly implemented sequences while discussing the implications of other potential configurations in the extended analysis.

Each category is further subdivided into six working conditions (A1–A3, B1–B3) according to the specific excavation order of the transverse passages. The detailed construction steps for all six conditions are listed in Table 4. Among them, A1 and B1 serve as representative working conditions and are used to investigate the dominant mechanisms governing the two construction systems.

Scheme A2: Based on A1, S-2 is excavated earlier, followed by S-1, L-2, and F-2.

Scheme A3: Based on A1, L-2 and F-2 are excavated first, followed by S-1 and S-2.

Scheme B2: Based on B1, S-2 is excavated earlier, followed by S-1, L-2, and F-2.

Scheme B3: Based on B1, L-2 and F-2 are excavated first, followed by S-1 and S-2.

Table 4: Construction sequences of Type A and Type B schemes

Step	Scheme A1	Scheme B1
1	Sheet pile construction	Construction of earth retaining walls
2	Excavate to the top floor of the structure, then construct the top floor	Excavation of temporary shaft 1
3	Backfill the excavated soil on the top floor to the surface	Construction of passage S-1 and inclined passage X-1
4	Excavate to the middle floor of the negative first floor, then construct the middle floor of the negative first floor	Excavation of temporary shaft 2
5	Excavate to the middle floor of the negative second floor, then construct the middle floor of the negative second floor	Construction of passage S-2, inclined passage X-2, and inclined passage X-3
6	Excavate to the designed bottom elevation, then construct the structure bottom floor	Excavation of temporary shaft 3

(Continued)

Table 4 (continued)

Step	Scheme A1	Scheme B1
7	Construction of passage S-1 and inclined passage X-1	Excavation of passage L-2 and F-2
8	Construction of passage S-2, inclined passage X-2, X-3	Excavation up to the structural roof, and construction of the roof
9	Excavation of passage L-2 and F-2	Backfilling of the excavated soil on the roof to the surface
10	/	Excavation up to the middle slab of the negative first floor, and construction of the middle slab of the negative first floor
11	/	Excavation up to the middle slab of the negative second floor, and construction of the middle slab of the negative second floor
12	/	Excavation up to the designed bottom elevation, and construction of the bottom slab of the structure

To characterize the deformation and internal-force responses of the existing station under different construction arrangements, schemes A1 and B1 are selected for detailed analysis, with horizontal comparisons across all six schemes. From the vertical and horizontal deformation contours and track-alignment deformation curves (Fig. 7), it is observed that the existing station undergoes overall upward heave. For all schemes, the maximum uplift appears below the S-1 passage, indicating that the soil disturbance is most severe at this location.

In Scheme A1, the deformation accumulates gradually throughout the construction process, with a final maximum uplift of 14.55 mm. In contrast, Scheme B1 exhibits a maximum uplift of only 10.45 mm, and its deformation curve displays a typical "inverted V-shape", demonstrating that constructing the mined passages first helps to partially offset the soil relaxation and rebound caused by subsequent foundation pit excavation. Both schemes show that the uplift of the right track is greater than that of the left track, indicating stronger unloading on the interchange-hall side and a certain degree of asymmetric deformation in plan view.

The accumulated horizontal displacements of the station base slab for the two schemes are shown in Fig. 8. Both schemes exhibit a typical "reverse coupling" deformation pattern: Mined passage excavation drives the station to move away from the foundation pit, whereas foundation pit excavation induces movement toward the pit. The final peak horizontal displacements are 3.35 mm for Scheme A1 and 0.75 mm for Scheme B1. The significantly smaller displacement in the B-type schemes indicates that the early formation of supporting structures helps restrain the lateral movement of the station.

The deformation and internal-force responses during the construction process are summarized in Table 5. The internal-force analysis further substantiates the above observations: In Scheme A1, local tensile stresses exceed the tensile strength of concrete, indicating a potential cracking risk. In Scheme B1, both compressive and tensile stresses remain within the allowable range, demonstrating a higher level of structural safety.

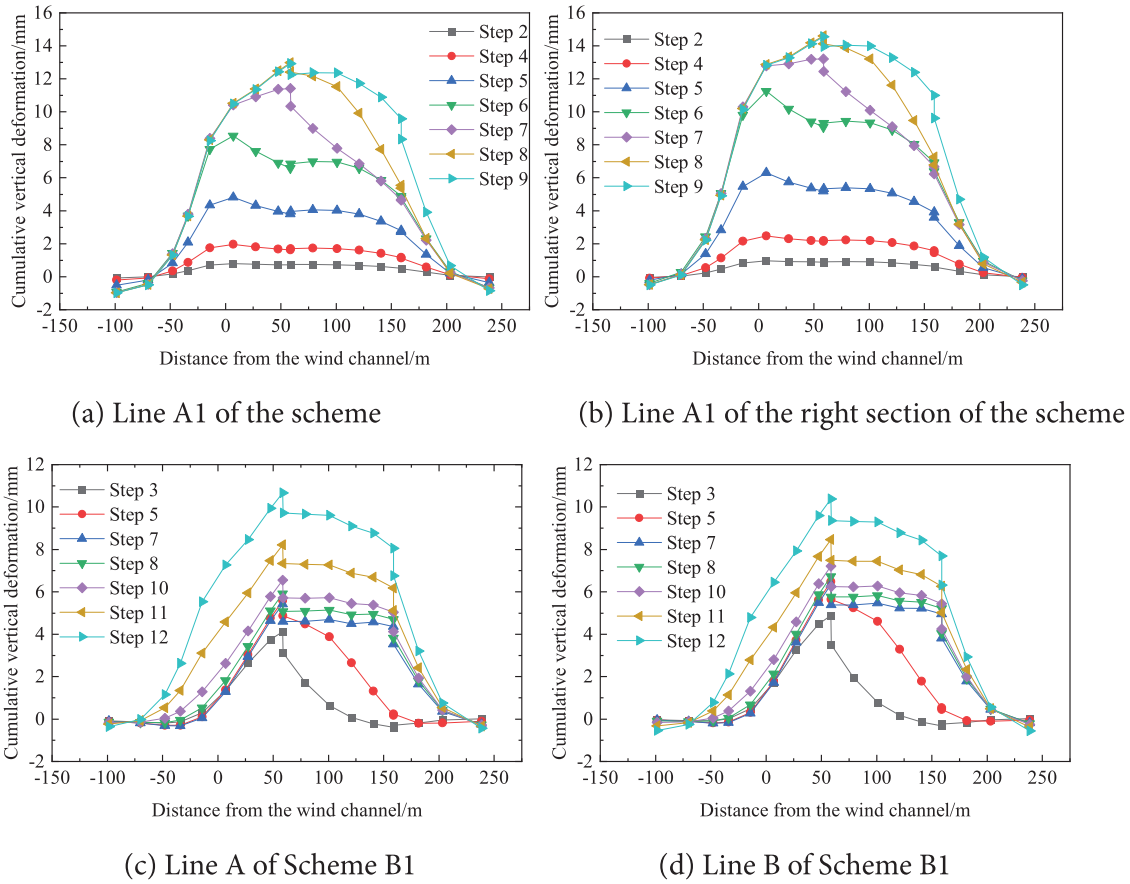

(a) Line A1 of the scheme

(b) Line A1 of the right section of the scheme

(c) Line A of Scheme B1

(d) Line B of Scheme B1

Figure 7: Cumulative vertical deformation of the existing station floor

The maximum vertical and horizontal deformation envelopes for both tracks during each construction stage are shown in Fig. 9. Type B schemes exhibit significantly smaller vertical and horizontal deformation than Type A schemes. The precise excavation order of the transverse passages has only a minor effect on the final deformation magnitudes. L-2 and F-2 produce the smallest uplift responses; S-1 induces the largest soil disturbance and corresponding deformation.

Overall, Type B schemes outperform Type A schemes in controlling vertical deformation, limiting horizontal displacement, and ensuring the safety of internal forces. The strategy of "constructing the mined passages first, followed by the foundation pit" provides a more effective staged mitigation of soil disturbance and significantly enhances the global stability of the existing metro station. Therefore, Type B schemes are recommended as the preferred construction approach for practical engineering implementation.

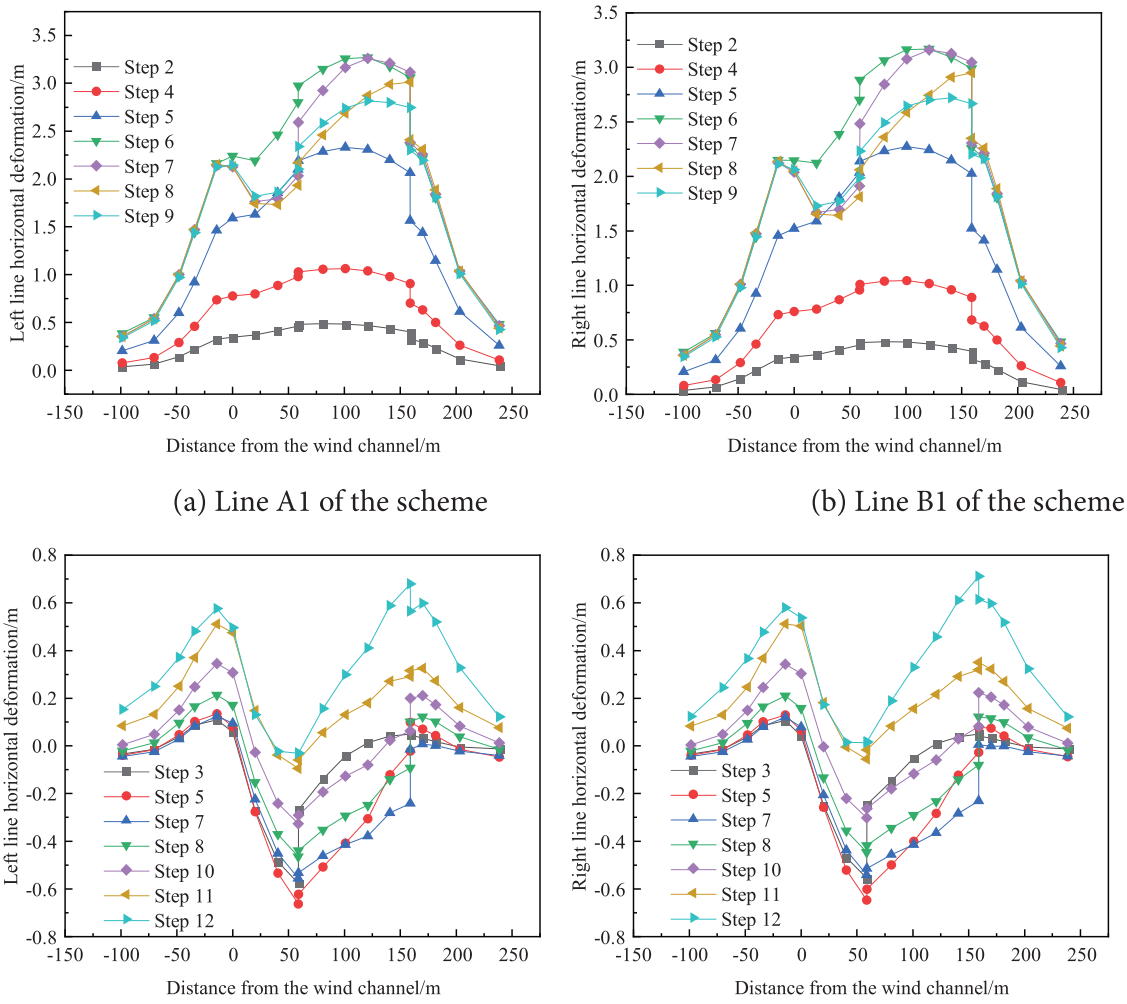

(a) Line A1 of the scheme

(b) Line B1 of the scheme

(c) Line A of Scheme B1

(d) Line B of Scheme B1

Figure 8: Cumulative horizontal deformation of the existing station floor

Table 5: Deformation and internal-force responses of the existing metro station

Project	A1	B1
Maximum vertical deformation/mm	+21.44	+11.31
Maximum horizontal deformation/mm	2.81	1.85
Maximum difference settlement of the deformation joint/mm	0.67	0.72
Maximum compressive stress/MPa	6.79	6.81
Maximum tensile stress/MPa	4.55	1.43

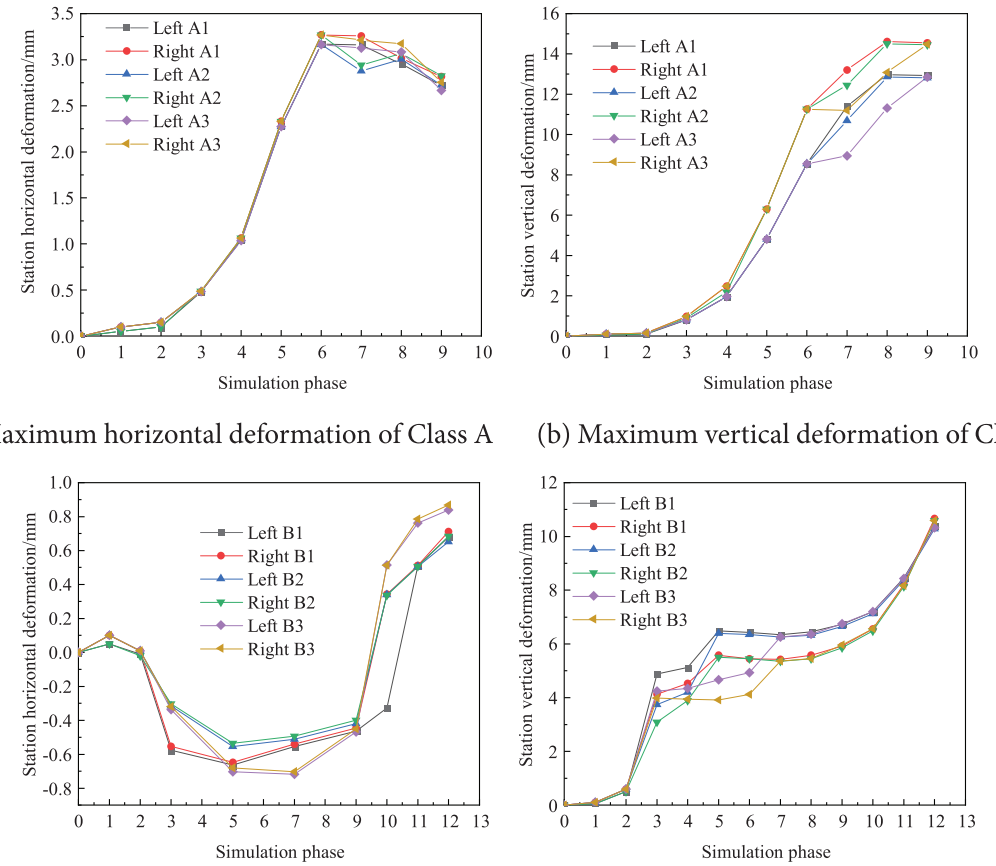

(a) Maximum horizontal deformation of Class A (b) Maximum vertical deformation of Class A

(c) Maximum horizontal deformation of Class B (d) Maximum vertical deformation of Class B

Figure 9: Variation of maximum deformation of different construction schemes

4.2 Response Characteristics of the Existing Station under Different Interlayer Thickness Conditions

In adjacent underground construction, the deformation and structural response of existing facilities are influenced not only by the construction method but also by the thickness of the intervening soil layer, the relative spatial arrangement between structures, and the stiffness of the underground components themselves. Based on the numerical model established in the previous section, this study investigates the combined effects of side-crossing tunnels, overcrossing passages, and parallel foundation pits on the existing station under varying clear-distance conditions. The objective is to clarify the response differences induced by changes in interlayer thickness and provide a basis for the safety management of closely spaced underground construction.

The spatial configuration is shown in Fig. 10. According to the engineering layout, three categories of clear-distance conditions are established. Horizontal interlayer thicknesses between the side-crossing tunnel and station are set to 1, 3, 5, 7, and 10 m. Vertical interlayer thicknesses between overcrossing passage and station are set to 0, 1, 3, 5, and 7 m. Horizontal interlayer thicknesses between the parallel interchange-hall foundation pit and station are set to 3, 5, 7, 10, and 15 m.

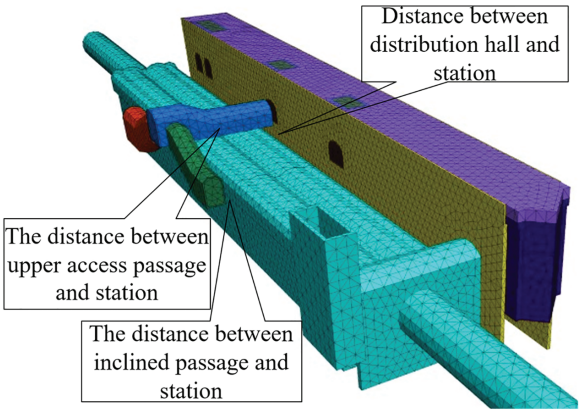

Figure 10: Spatial relationship among the station, interchange hall, and tunnels

For each condition, an independent numerical model is constructed, and the maximum vertical and horizontal deformations of the existing station are extracted. The results are shown in Figs. 11–13. As the horizontal clear distance between the inclined tunnel and the station increases from 1 to 5 m, both vertical and horizontal deformations of the station decrease significantly. However, when the clear distance exceeds 7 m, the rate of deformation reduction decreases noticeably. Within the close-range zone (<5 m), the station response is highly sensitive to lateral disturbance; Beyond a certain threshold (>5 m), stress attenuation with distance causes the marginal benefit of increasing clear distance to diminish.

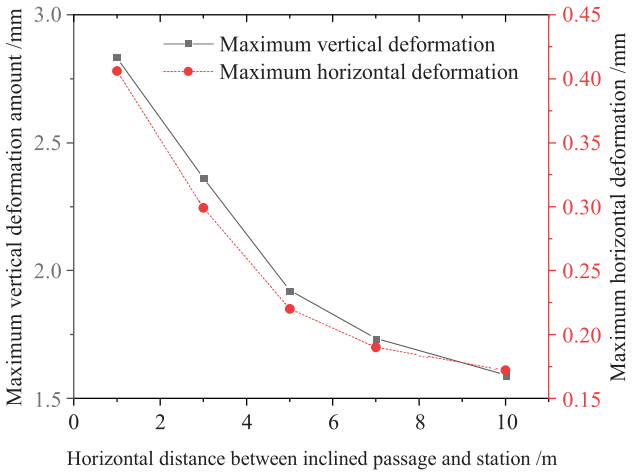

Figure 11: Maximum station deformation under different horizontal distance between inclined passage and station

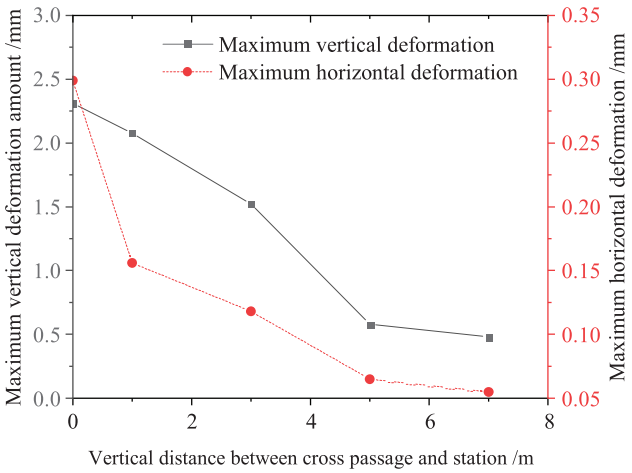

Figure 12: Maximum station deformation under different vertical distance between cross passage and station

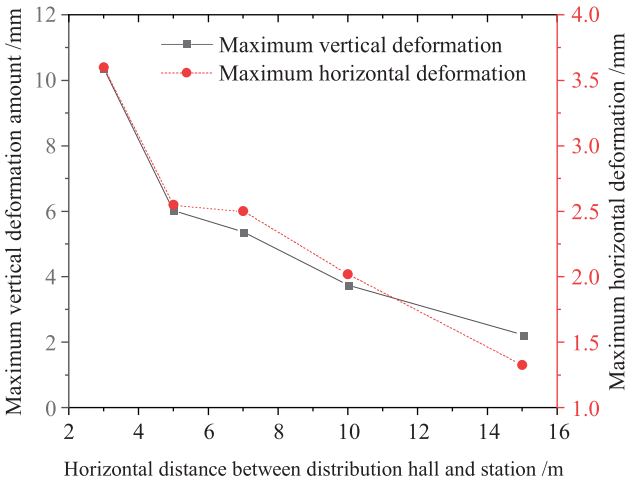

Figure 13: Maximum station deformation under different horizontal distance between distribution hall and station

With increasing vertical soil thickness between the overcrossing passage and the station, both the uplift and horizontal displacement of the existing station decrease markedly. The most significant deformation reduction occurs when the interlayer thickness increases from 0 to 3 m, while further increases to 5–7 m result in progressively smaller improvements. A thicker vertical soil layer provides: greater overburden stress, higher global stiffness, stronger confinement, which together better resist uplift or unloading caused by tunnel excavation. Once the vertical clear distance reaches a certain level, the stress-interference zone stabilizes, and continuing to increase the thickness yields limited additional benefit.

To compare the effect of different construction types under fixed clear distances, a 4 m increase in horizontal or vertical separation results in the following reductions in maximum station deformation: Side-crossing tunnel: deformation decreased by 35.7%, Overcrossing passage: deformation decreased by 60%, Parallel foundation pit: deformation decreased by 50%. It should be noted that these values are not formal sensitivity indices, but rather indicate the relative effectiveness of clear-distance increases in controlling station deformation under the selected conditions. Across all three construction types, increasing the horizontal or vertical separation consistently mitigates deformation, while beyond the threshold distances,

the marginal benefit of further separation becomes limited. These results provide guidance for construction scheme optimization and safety control under complex adjacent construction scenarios.

4.3 Influence of Passageway Location on the Deformation Response of the Existing Station

To investigate the deformation behavior of the existing station under different spatial arrangements of overcrossing and inclined passages, numerical simulations are conducted for the S-2, X-2, and X-3 passages at various longitudinal positions. Given that the existing station has a total interval length of L = 180 m, the passage locations are set at L/4, L/2, 3L/4, and at the expansion joint, as illustrated in Fig. 14.

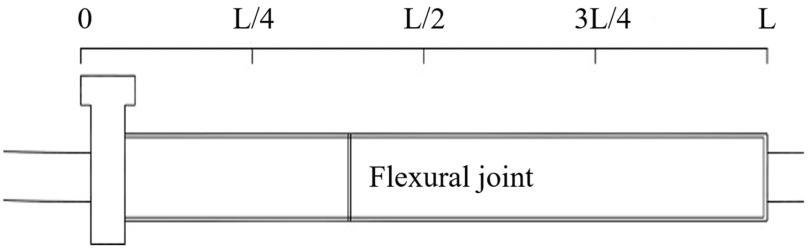

Figure 14: Schematic layout of the transverse passages in the existing station

Three-dimensional numerical models are established for each working condition, and the computed results are shown in Fig. 15. The curves represent the vertical deformation along the left and right track slabs, while the contour plots illustrate the cumulative vertical deformation of the station (magnified 500 times) together with the relative spatial relationship between the passage and the station. The results indicate that the location of the passageway has a pronounced impact on both the magnitude and the spatial extent of vertical deformation. When the passage is located near the expansion joint, the vertical deformation reaches its maximum, followed by the 3L/4 and L/4 positions, whereas the mid-span (L/2) location results in the smallest deformation. Overall, the station exhibits a typical "single-trough" uplift pattern.

This behavior is attributed to the spatial variability of structural stiffness: The central portion of the station features relatively high stiffness, providing stronger resistance to vertical displacement; The end regions, where the station interfaces with the shield-driven tunnels, exhibit lower stiffness, making them more susceptible to localized deformation under disturbance; Consequently, the expansion-joint region, with inherently reduced stiffness, shows the largest deformation response.

The influence extent of the disturbance also varies with the passage position: construction at the 3L/4 and L/4 positions produces wider affected zones, whereas the expansion joint and L/2 positions generate more localized responses. This pattern aligns with the stiffness distribution along the station, where higher-stiffness central regions limit deformation propagation, while lower-stiffness ends facilitate wider influence zones. Differences are also observed between the two track lines: the right track experiences larger vertical deformation amplitudes but within a relatively smaller affected area compared with the left track. This is mainly governed by the relative spatial positioning between the passage and the station, which leads to uneven stress concentration and different deformation transmission paths. To effectively control the deformation of the existing station, it is recommended to avoid placing the passageway near the expansion joint. Positioning the passage within the central high-stiffness region is preferable, as it reduces both the deformation magnitude and the disturbance range. These findings offer valuable guidance for passageway layout planning and construction organization in closely adjacent underground engineering.

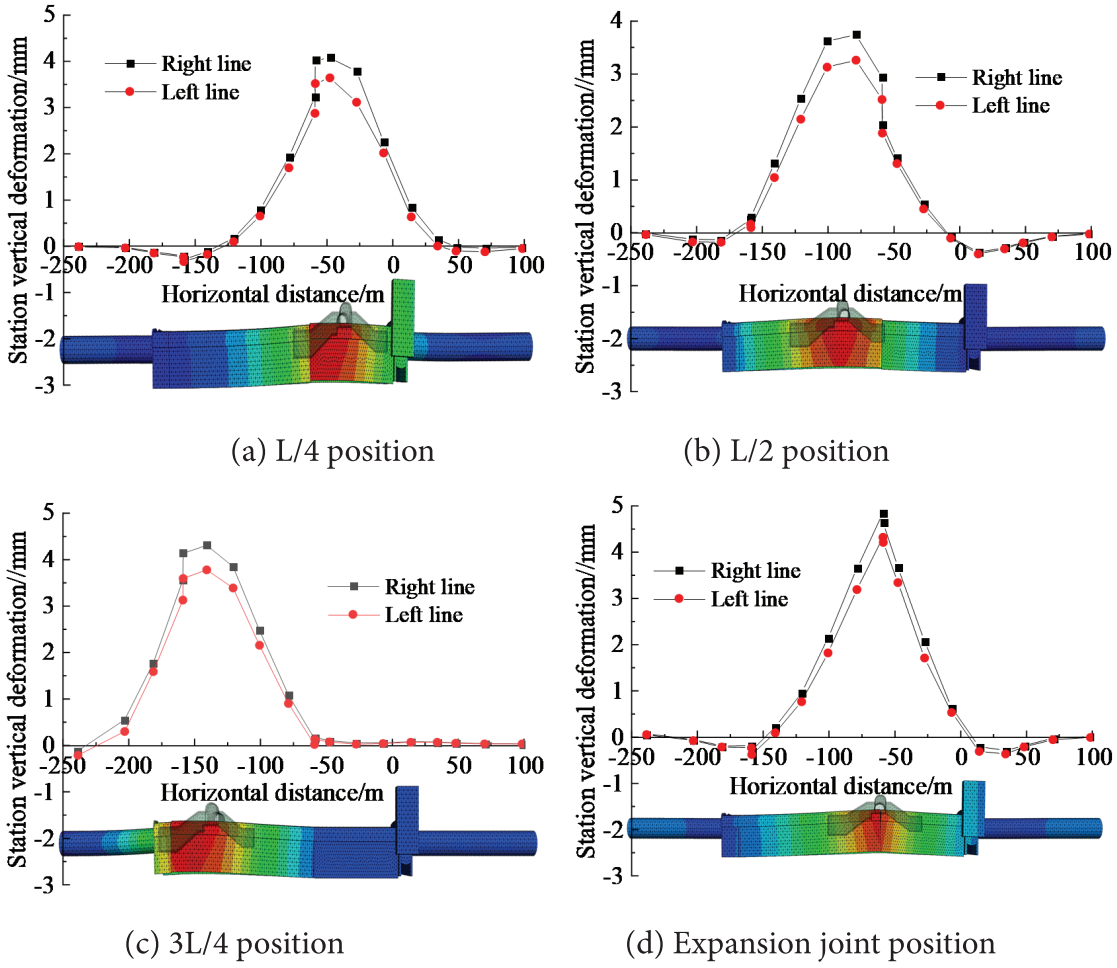

Figure 15: Vertical deformation curves of the existing station for different passage locations

The maximum principal stress of the existing station for different passage locations is shown in Fig. 16. When the passage is located at the expansion-joint region, the excavation-induced stress variation in the station structure remains relatively small due to the joint's deformation-accommodating characteristics.

The horizontal deformation curves of the existing station under different passage locations are presented in Fig. 17. The maximum horizontal displacements at the L/4, L/2, 3L/4, and expansion-joint positions are 0.038, 0.034, 0.049, and 0.058 mm, respectively. The expansion-joint region exhibits the largest deformation; however, its deformation also attenuates the fastest with increasing distance from the disturbance.

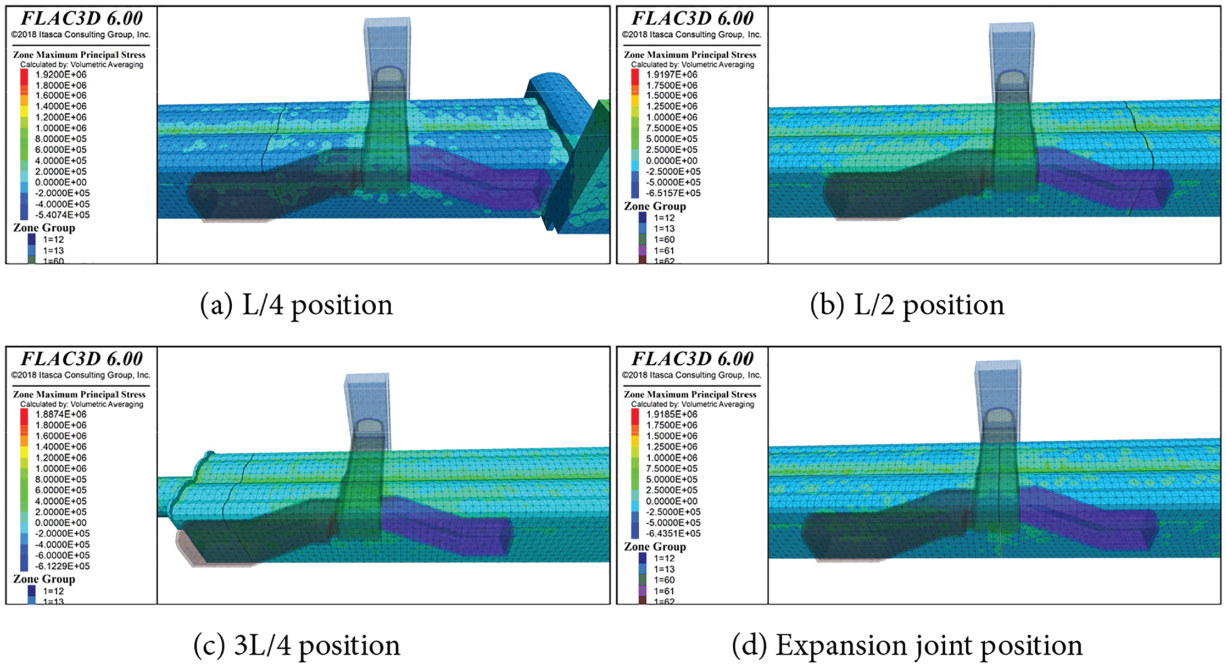

Figure 16: Maximum principal stress of the existing station for different passage locations

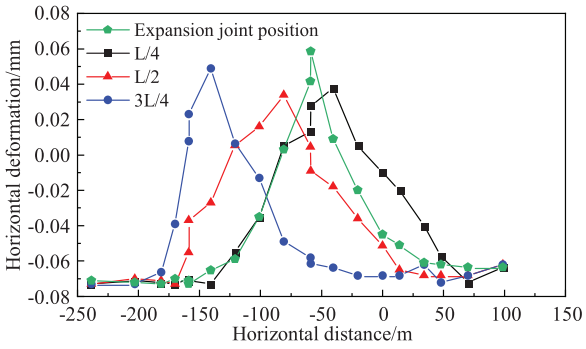

Figure 17: Horizontal deformation curves of the existing station for different passage locations

5 Conclusions

This study analyzed the deformation response and structural behavior of an existing metro station under various construction conditions, such as different sequences, interlayer thicknesses, and passageway layouts. By using detailed three-dimensional numerical models, the research identified the disturbance mechanisms from adjacent deep excavations, side-crossing and overcrossing passages, and provided targeted strategies for effective engineering design and construction.

(1) The construction order exerts a significant effect on station deformation. When transverse passages are constructed before the interchange hall excavation, the maximum vertical and horizontal deformations are limited to 11.31 and 1.85 mm. Reversing the sequence increased these values to 21.44 and 2.81 mm. This demonstrates that early construction of the passages forms a portal-frame stiffening effect that effectively reduces structural deformation.

(2) The station mainly experienced uplift, with the maximum vertical displacement of 4.99 mm occurring near the S-1 passage expansion joint, while the corresponding horizontal displacement reached approximately 1.45 mm. The excavation of inclined passages produced the strongest disturbance, indicating that this stage requires the most stringent monitoring and deformation control measures.

(3) The position of the passageways noticeably affected both the magnitude and spatial distribution of station deformation. The greatest vertical displacement occurred at the expansion-joint region, followed by the 3L/4 and L/4 locations, whereas the mid-span (L/2) produced the smallest response. Deformation propagation is widest at 3L/4 and L/4, while the expansion-joint and mid-span conditions showed more localized influence. Therefore, positioning new passages away from expansion joints and closer to the central span can help minimize deformation due to the higher longitudinal stiffness in this region.

This study, based on the Gaojiayuan Station case, systematically investigates the deformation and structural response of an existing metro station under simultaneous construction of a new foundation pit and adjacent mined passages. The findings highlight the influence mechanisms of lateral and vertical clear distances, longitudinal stiffness distribution, and construction sequences. However, the quantitative thresholds and sensitivity levels obtained herein are dependent on the specific geological conditions, structural configuration, and construction methods adopted in this case. Future research should therefore expand validation efforts to a broader range of geotechnical environments—such as highly saturated soft clays, dense sand layers, and stiff silty soils—as well as different existing-station structural types and surrounding rock classes, to establish more generalizable deformation attenuation patterns and clear-distance thresholds.

Acknowledgement: None.

Funding Statement: The authors gratefully acknowledge the financial support by the National Natural Science Foundation of China (Project No. U2469207, received by Qian Fang) and Science and Technology Innovation Program of Xiongan New Area (Project No. 2024XAGG0016, received by Qian Fang).

Author Contributions: The authors confirm contribution to the paper as follows: study conception and design: Jun Wang, Qian Fang; data collection: Weiguo He, Yanxin Chen; analysis and interpretation of results: Jun Wang, Qizhao You; draft manuscript preparation: Jun Wang, Qian Fang, Weiguo He. All authors reviewed the results and approved the final version of the manuscript.

Availability of Data and Materials: The data and materials in the current study are available from the corresponding author on a reasonable request.

Ethics Approval: Not applicable.

Conflicts of Interest: The authors declare no conflicts of interest to report regarding the present study.

References

1. Wu B, Liu W, Shi P, Xu X, Liu Y. A case study of newly tunnels over-crossing the existing subway tunnels. Int J Distrib Sens Netw. 2022;18(3):155013292210871. doi:10.1177/15501329221087183.
2. Akbarzadeh Arpachaei M, Jalali SE, Khademian A. Determining the best depth of subway tunnel excavation considering ground type, support system characteristics, and tunneling cost: case study of Tabriz subway, Line 2. Bull Eng Geol Environ. 2023;82(11):423. doi:10.1007/s10064-023-03448-1.
3. Liu Y, Zhang M, Li P, Zhou A, Wang L, Xu H. Bending performance of Y-shaped joints of subway station built by enlarging two parallel shield tunnels. Tunn Undergr Space Technol. 2023;142:105427. doi:10.1016/j.tust.2023.105427.
4. Barski ES, Hong DL. Design of deep-buried subway station in Moscow. Tunn Undergr Sp Tech. 2000;1:33–9.

5. Wu J, Ma S, Wang R, Ou F, Liang Y, Zhao W, et al. A novel technique for constructing prefabricated subway stations under open excavation. Proc Inst Civ Eng Eng Sustain. 2024;177(5):299–308. doi:10.1680/jensu.23.00015.
6. Zhang JL, Gao YM, Liu X, Zhang ZA, Yuan Y, Mang HA. A shield tunneling method for enlarging the diameter of existing tunnels: experimental investigations. Tunn Undergr Space Technol. 2022;128:104605. doi:10.1016/j.tust.2022.104605.
7. Liu J, Qi T, Wu Z. Analysis of ground movement due to metro station driven with enlarging shield tunnels under building and its parameter sensitivity analysis. Tunn Undergr Space Technol. 2012;28:287–96. doi:10.1016/j.tust.2011.12.005.
8. Hu H, Zhang Y, Yang G, Zhong Z, Chen F. Measurement and numerical analysis of effect of excavation of foundation pits on metro tunnels. Chin J Geotech Eng. 2014;36(S2):431–39. (In Chinese). doi:10.11779/CJGE2014S2075.
9. Ling T, Wu X, Huang F, Xiao J, Sun Y, Feng W. Optimization of construction support scheme for foundation pits at zero distance to both sides of existing stations based on the pit corner effect. Geomech Eng. 2024;38(4):381–95. doi:10.12989/gae.2024.38.4.381.
10. Qiu Y, Wang J, Zhang C, Hua L, Zhou Z. Numerical simulation study on the impact of excavation on existing subway stations based on BIM-FEM framework. Buildings. 2024;14(5):1444. doi:10.3390/buildings14051444.
11. Dai J. Monitoring and deformation analysis of adjacent existing subway facilities influenced by deep foundation pit excavation. Hans J Civ Eng. 2022;11(8):954–62. doi:10.12677/hjce.2022.118103.
12. Dong X, Mei L, Yang S, He L. Deformation response research of the existing subway tunnel impacted by adjacent foundation pit excavation. Adv Mater Sci Eng. 2021;2021:5121084. doi:10.1155/2021/5121084.
13. Ma B, Wu S, Chen Q, Liang E, Li X. The influence of existing piles on station settlement during the construction of a tunnel undercrossing under existing stations. Sci Rep. 2024;14(1):14024. doi:10.1038/s41598-024-63921-z.
14. Wu S, Zhang X, Lin Z, Wang J, Zhang F, Gao H. Influence law and determination method of jack lifting load on existing station settlement. Case Stud Constr Mater. 2025;22:e04180. doi:10.1016/j.cscm.2024.e04180.
15. Zhu F, Huang H, Liu X, Liu H, Dai Z. Influence of large foundation pit excavation on adjacent subway tunnel. Destech Trans Eng Technol Res. 2018. doi:10.12783/dtetr/iccere2017/18273.
16. liu B, Wu W, Lu H, Chen S, Zhang D. Effect and control of foundation pit excavation on existing tunnels: a state-of-the-art review. Tunn Undergr Space Technol. 2024;147:105704. doi:10.1016/j.tust.2024.105704.
17. Zhang Y, Yi L, Zhang L, Yang Y, Hao X, Li H, et al. Causation identification and control measures of deformation by integrated dewatering-excavation process simulation of a T-shaped deep foundation pit. Water. 2022;14(4):535. doi:10.3390/w14040535.
18. Yu C, Long J, Lu M. Study on the influence of deep foundation pit excavation on adjacent metro structure. IOP Conf Ser: Earth Environ Sci. 2021;768(1):012101. doi:10.1088/1755-1315/768/1/012101.
19. Yang T, Xiong S, Liu S, Liu Y, Zhao H, Li Y. Numerical analysis of the influence of deep foundation pit construction on adjacent subway stations in soft soil areas. Adv Civ Eng. 2022;2022:6071868. doi:10.1155/2022/6071868.
20. Zhou F, Zhou P, Li J, Lin J, Ge T, Deng S, et al. Deformation characteristics and failure evolution process of the existing metro station under unilateral deep excavation. Eng Fail Anal. 2022;131:105870. doi:10.1016/j.engfailanal.2021.105870.
21. Qiu JT, Jiang J, Zhou XJ, Zhang YF, Pan YD. Analytical solution for evaluating deformation response of existing metro tunnel due to excavation of adjacent foundation pit. J Cent South Univ. 2021;28(6):1888–900. doi:10.1007/s11771-021-4737-3.
22. Wang J, Geng D, Luo Z, Zhao J, Liu X, Zong H, et al. Real-time prediction system for tunnel deformation induced by excavation and its application. Sci Prog. 2025;108(2):368504251349975. doi:10.1177/00368504251349975.
23. Avgerinos V, Potts DM, Standing JR. Numerical investigation of the effects of tunnelling on existing tunnels. Géotechnique. 2017;67(9):808–22. doi:10.1680/jgeot.sip17.p.103.
24. Huang Z, Zhang C, Fu H, Deng H, Ma S, Fu J. Numerical study on the disturbance effect of short-distance parallel shield tunnelling undercrossing existing tunnels. Adv Civ Eng. 2020;2020:8810658. doi:10.1155/2020/8810658.
25. Yang F, Liu J, Liu Y, Zhang L. Research on spacing effect of the construction of shield tunnels undercrossed existing tunnels at close distance. IOP Conf Ser Earth Environ Sci. 2018;189:022086. doi:10.1088/1755-1315/189/2/022086.

26. Ou X, Liu Y, Li C, Zhou X, Chen Q, Zhou Y, et al. Analysis of the interaction effects of shield structure oblique passing under an existing tunnel. Appl Sci. 2022;12(11):5569. doi:10.3390/app12115569.
27. Fu YM, Ding WQ, Qiao YF. Impact of small-angle shield undercrossing on existing tunnels. IOP Conf Ser Earth Environ Sci. 2024;1333(1):012057. doi:10.1088/1755-1315/1333/1/012057.
28. Wei X, Zhang M, Ma S, Xia C, Liu X, Ding Z. Deformation characteristics of existing twin tunnels induced by double shield undercrossing with prereinforcement: a case study in Hangzhou. Adv Civ Eng. 2021;2021:7869899. doi:10.1155/2021/7869899.
29. Ahmed NZ, El-Shourbagy M, Akl A, Metwally K, Choudhary AK. Field monitoring and numerical analysis of ground deformation induced by tunnelling beneath an existing tunnel. Cogent Eng. 2021;8(1):1861731. doi:10.1080/23311916.2020.1861731.
30. Fu C, Gao Y. Numerical analysis on the behavior of existing tunnels subjected to the undercrossed shield tunneling at a small proximity. Adv Civ Eng. 2020;2020:8823331. doi:10.1155/2020/8823331.
31. Wu S, Shi J, Wu J, Li L, Jin H. Risk factor recognition of shield tunnel crossing underneath the existing subway tunnel. IOP Conf Ser Earth Environ Sci. 2021;676(1):012134. doi:10.1088/1755-1315/676/1/012134.
32. Zhou Z, Zhou Y, Zhang H, Chen S, Xiang L, Wang L. Effects of foundation excavation on metro tunnels at different locations and performance of corresponding reinforcement measures: a case of Shenzhen metro line 11, China. Symmetry. 2022;14(12):2561. doi:10.3390/sym14122561.
33. Lu C, Huang L. Study on the effect of foundation pit excavation on the deformation of adjacent shield tunnel. Adv Civ Eng. 2022;2022:8441758. doi:10.1155/2022/8441758.
34. Liu B, Lin H, Chen Y, Liu J, Guo C. Deformation stability response of adjacent subway tunnels considering excavation and support of foundation pit. Lithosphere. 2022;2022(Special 10):7227330. doi:10.2113/2022/7227330.
35. Wei G, Mu Z, Feng W, Qi Y, Guo B. Effects of foundation pit excavation on adjacent metro stations and shield tunnel structures: a study on horizontal displacement. Eng Comput. 2024;41(10):2356–80. doi:10.1108/ec-06-2024-0543.
36. Huang X, Schweiger HF, Huang H. Influence of deep excavations on nearby existing tunnels. Int J Geomech. 2013;13(2):170–80. doi:10.1061/(asce)gm.1943-5622.0000188.
37. Wang H, He S. Stability analysis of surrounding rock of shallow-buried subway tunnel with small spacing under different working conditions. Geotech Geol Eng. 2022;40(10):5065–79. doi:10.1007/s10706-022-02200-y.